Int J Earth Sci (Geol Rundsch) (2011) 100:1163–1179
DOI 10.1007/s00531-010-0626-y

ORIGINAL PAPER

Cosmogenic ^{10}Be-derived denudation rates of the Eastern and Southern European Alps

Kevin P. Norton · Friedhelm von Blanckenburg · Roman DiBiase · Fritz Schlunegger · Peter W. Kubik

Received: 8 January 2010 / Accepted: 13 November 2010 / Published online: 5 January 2011

Abstract Denudation rates from cosmogenic ^{10}Be measured in quartz from recent river sediment have previously been used in the Central Alps to argue that rock uplift occurs through isostatic response to erosion in the absence of ongoing convergence. We present new basin-averaged denudation rates from large rivers in the Eastern and Southern European Alps together with a detailed topographic analysis in order to infer the forces driving erosion. Denudation rates in the Eastern and Southern Alps of 170–1,400 mm ky^{-1} are within a similar range to those in the Central Alps for similar lithologies. However, these denudation rates vary considerably with lithology, and their variability generally increases with steeper landscapes, where correlations with topographic metrics also become poorer. Tertiary igneous rocks are associated with steep hillslopes and channels and low denudation rates, whereas pre-Alpine gneisses usually exhibit steep hillslopes and higher denudation rates. Molasse, flysch, and schists display lower mean basin slopes and channel gradients, and, despite their high erodibility, low erosion rates. Exceptionally low denudation rates are also measured in Permian rhyolite, which has high mean basin slopes. We invoke geomorphic inheritance as a major factor controlling erosion, such that large erosive glaciers in the late Quaternary cold periods were more effective in priming landscapes in the Central Alps for erosion than in the interior Eastern Alps. However, the difference in tectonic evolution of the Eastern and Central Alps potentially adds to differences in their geomorphic response; their deep structures differ significantly and, unlike the Central Alps, the Eastern Alps are affected by ongoing tectonic influx due to the slow motion and rotation of Adria. The result is a complex pattern of high mountain erosion in the Eastern Alps, which has evolved from one confined to the narrow belt of the Tauern Window in late Tertiary time to one affecting the entire underthrust basement, orogenic lid, and parts of the Southern Alps today.

Keywords Cosmogenic nuclides · Denudation rates · European Alps · Orogenic steady state

K. P. Norton (✉) · F. von Blanckenburg
Institute for Mineralogy, Leibniz University of Hannover, Hanover, Germany
e-mail: norton@geo.unibe.ch

R. DiBiase
School of Earth and Space Exploration, Arizona State University, Tempe, AZ, USA

Present Address:
K. P. Norton · F. Schlunegger
Institute of Geological Sciences, University of Bern, Bern, Switzerland

P. W. Kubik
Laboratory for Ion Beam Physics, ETH Zurich, Zurich, Switzerland

Present Address:
F. von Blanckenburg
German Research Center for Geosciences GFZ, Potsdam, Germany

Introduction

The surface expression of a mountain range is a result of the interplay of elevation gains through convergence and elevation loss through erosion or tectonic exhumation. During the initial phases of orogen growth, high mass flux into the range results in an increase in the thickness of the crust above its base and, in a second phase through isostatic

compensation, also resulting in an increase in the relief of the range (Stüwe and Barr 1998). During this second stage, the excess in gravitational energy accrued during thickening (Molnar and Lyon-Caen 1988) can lead to lateral escape (Tapponnier et al. 1986) or orogenic collapse (Dewey 1988). Because an increase in topographic relief typically also results in an increase in denudation rates by fluvial incision, rock weathering, mass wasting, and glacial erosion, any further mass flux into the range is increasingly balanced by denudation (Willett et al. 2001). During this phase of active convergence, limits on attainable slopes and relief lead to a steady state between lithospheric and surface mass flux (Willett and Brandon 2002; Willett et al. 2001), such that changes in rock uplift rates are compensated by an equivalent change in denudation rate. Therefore, denudation rates at this stage depend on the tectonic flux entering the system. Cessation of convergence leads to a decay in orogen development, during which the thick crustal root responds isostatically to erosion. During this decay, climate drives crustal thinning through erosion (England and Molnar 1990). Some important terminology is associated with these concepts (England and Molnar 1990; Stüwe and Barr 1998): "Rock uplift" is defined as the vertical motion of rock relative to a reference level, usually taken to be the geoid. "Denudation" is the removal of material from the surface, either by a combination of erosion and weathering (erosional denudation) or by tectonic processes (tectonic denudation). "Exhumation" is movement of rock relative to the surface (England and Molnar 1990; Stüwe and Barr 1998), whereas "surface uplift" is the change in the vertical position of the surface relative to the reference level and is the difference between rock uplift and denudation or exhumation, i.e., surface uplift = rock uplift − denudation. Importantly, in both the steady and decaying states of orogenesis, denudation rate correlates positively with rock uplift rate (Stüwe and Barr 1998).

The European Alps are one of the few mountain belts for which an exceedingly high density of geologic data allows the differentiation of the various modes of orogenic development. The Western Alps is arguably the only part of the orogen where orogenic collapse may be occurring today (Selverstone 2005). In the Central and Eastern Alps, normal and strike-slip faults oriented at a high angle to orogen trend were active primarily in the middle Tertiary (Ratschbacher et al. 1989; Mancktelow 1992). Subsequently, during the late Tertiary, exhumation in the Eastern Alps was focused within the narrow Tauern Window, whereas in the Western and Central Alps exhumation was distributed over a much wider area. This led Rosenberg and Berger (2009) to suggest that changes in the deep structure and rheology of the Alps exerted a prime control on its lateral growth (Rosenberg and Berger 2009). Late Tertiary and Quaternary sediment budgets (Kuhlemann et al. 2002) and fission-track age compilations (Vernon et al. 2008) indicate a climate-driven acceleration of sedimentation rates (Kuhlemann et al. 2002; Schlunegger and Simpson 2002; Cederbom et al. 2004; Willet et al. 2006, and review by Willett 2010). However, this view of climate-driven increases in erosional efficiency has been challenged based on steady detrital zircon-derived exhumation rates of the Alps over the past 10 My (Bernet et al. 2009), and on the absence of a weathering signal in authigenic marine $^{10}Be/^{9}Be$ ratios (Willenbring and von Blanckenburg 2010). Most present-day tectonic activity in the Eastern Alps is localized on strike-slip faults that accommodate lateral extrusion of the orogenic crust (rather than orogenic collapse) that has been driven at least in part by eastward tectonic escape during N–S- to NNE–SSW-directed convergence of the Adriatic microplate with Europe (Ratschbacher et al. 1989, 1991; Robl and Stüwe 2005; Robl et al. 2008b; Rosenberg et al. 2007).

New studies of the late Holocene to recent denudation rates in the Alps using cosmogenic nuclides in sediment from large Alpine rivers (Wittmann et al. 2007; Norton et al. 2008; Delunel et al. 2010), rock uplift rates by leveling (Kahle et al. 1997; Schlatter et al. 2005; Ruess and Höggerl 2002), and convergence rates by GPS (Battaglia et al. 2004; Calais et al. 2002; Weber et al. 2010) have provided a wealth of data pertaining to surface processes in the Alps, allowing us further to constrain these contradicting models in an unprecedented way. The patterns and magnitude of denudation in the Central and Western European Alps match My exhumation rates (Vernon et al. 2009; Wittmann et al. 2007) as well as modern rock uplift rates in the Central Alps (Kahle et al. 1997; Schlatter et al. 2005; Wittmann et al. 2007). For the late Holocene Central Alps, the most important observation is the correlation between cosmogenic nuclide-derived denudation rate and rock uplift rate (Wittmann et al. 2007). Both these parameters are highest where altitude, relief, and crustal thickness are highest. This might indicate a steady-state relationship between uplift and denudation in which uplift is driven by denudation (Wittmann et al. 2007). This hypothesis is supported by the observation that there is no active convergence in the Central Alps detectable by GPS (Grenerczy et al. 2005) and that convergence between Adria and Europe dropped to values of 0.5 mm $year^{-1}$ or less some 20 Ma (Fig. 16 in Handy et al. 2010 and references therein). It also corroborates the results of a 2D model of denudation-driven rock uplift of the Central Alps (Champagnac et al. 2009).

In this study, we extend the Alpine dataset of ^{10}Be-based denudation rates to the Eastern and Southern Alps where erosion–uplift–lithology relationships have remained largely unexplored. We focus on this part of the Alps because

recent studies point to strong differences between the Eastern and Central Alps in surface morphology (Robl et al. 2008a) and tectonic setting (Rosenberg and Berger 2009). Specifically, the Eastern Alps still retain their orogenic lid of Austroalpine nappes including their Mesozoic sedimentary cover, suggesting that Neogene time-integrated erosion and exhumation rates may be significantly lower than in the Central Alps. This lid has been removed above a narrow zone of exhumation only from the Tauern Window. ^{10}Be-derived denudation rates allow us to determine whether this tectonic pattern has prevailed in the Holocene or whether climatic changes have reset rates of denudation.

Geographic and geological setting

The European Alps are readily separated into the Eastern, Central, Western, and Southern sections on both geodynamic and lithologic grounds (e.g., Schmid et al. 2004). A marked feature of the Alps shown in Fig. 1 are deeply eroded, crystalline basement rocks of lower-plate (European) origin that are exposed in the external massifs (e.g., Aar, Pelvoux, Mont Blanc massifs) and the Penninic cores regions of the Central Alps (Lepontine) and Eastern Alps (Tauern). These units underlie nappes comprising Permo-Mesozoic rocks derived from the Helvetic (European margin) and Penninic paleogeographic realms of the Alpine Tethyan Ocean (Handy et al. 2010). To the east, the Penninic crystalline basement, including the metamorphic and sedimentary cover of European origin and of the Alpine Tethyan Ocean, is well exposed only in the antiformal stack of the Tauern Window. In the Central and Western Alps, the Penninic basement core is flanked by externally vergent thrust sheets to the north and west (Helvetic, Penninic) and by the south-vergent thrust sheets of the Southern Alpine units. These units are bordered by peripheral foreland basins (the Oligo-Miocene Molasse basin in the north and the Mio-Pliocene Po Basin in the south). Most of the Eastern Alps are covered by the NW- and W-thrusted Austroalpine nappes making up the orogenic lid. These nappes consist consisting of pre-Alpine basement rocks and their Paleozoic and Mesozoic sedimentary cover, which were thrusted and metamorphosed already during the late Cretaccous Eo-alpine orogeny (e.g., Schmid et al. 1996, 2004; Handy et al. 2010). Late Tertiary movement along the Insubric or Periadriatic Fault System resulted in exposure of the high-grade Penninic crystalline core of the Lepontine dome and the Tauern Window (Schmid et al. 1989; Handy et al. 2005). This Oligo-Miocene Insubric tectonics was also associated with the emplacement of mainly tonalitic and granodioritic melt into the retro-wedge of the Alpine orogen, including the Bergell and Adamello plutons (Schmid et al. 1996; von Blanckenburg et al. 1998).

In the present Central Alps, the European lithosphere descends to the S and SW beneath the Adriatic plate (Schmid and Kissling 2000; Persaud and Pfiffner 2004). The European Moho depth as imaged by reflection seismology in the NFP-20 section is 30 km to the north of the Central Alps increasing to ca. 50 km beneath the Central Alps, then decreasing again to ca. 35 km beneath the southern Central Alps. South of the Central Alps, the Adriatic Moho is shallow (ca. 20 km) due to Tertiary northward wedging of the Adriatic lower crust, and its near surface expression, the Ivrea geophysical body (Schmid et al. 2004). Beneath the "Transalp" seismic profile in the Eastern Alps, the European Moho is imaged by both reflection seismic and receiver functions to dip gently southward, from a depth of 35 km beneath the northern foreland to a maximum depth of 55 km beneath the central part of the Eastern Alps. In contrast, the Adriatic Moho is imaged by the receiver function method to be at a relatively constant depth of about 40 km (Kummerow et al. 2004). A south-directed subduction of European lithosphere was also reconstructed for the entire Eastern Alps (Brückl et al. 2010), contrary to the northward subduction of the Adriatic plate beneath the European plate since late Oligocene to Miocene time as has been suggested (Schmid et al. 2004) based on mantle tomography (Lippitsch et al. 2003). Throughout this paper, we assume that the base of the crust is the isostatic compensation depth.

The location of deformation in the Eastern Alps appears to have shifted southwards by more than 150 km since the late Miocene (Rosenberg and Berger 2009). In the Eastern Alps, GPS solutions indicate N–S shortening 100 km to the south of the Periadriatic lineament with little to no shortening to the north of this tectonic line (Grenerczy et al. 2005). However, based on seismic records and the existence of deformed gravels (Neubauer et al. 2007), it is likely that movement on the northern flank of the Tauern Window is still occurring. The recent tectonics in the Eastern Alps are associated with a counterclockwise rotation of the Adriatic plate with respect to the European plate with the pole of rotation centered within the arc of the Western Alps (Fig. 1; Battaglia et al. 2004; Calais et al. 2002; Weber et al. 2010). Thus, convergence in the Central Alps is immeasurably small, while N–S to NE–SW-directed convergence rates of $\sim$2 to 4 mm year^{-1} are accommodated across the Southern Alps south of the Tauern Window (Vrabec et al. 2006).

Modern Alpine topography has been sculpted by Quaternary glaciation, most recently during the last glacial maximum (LGM) (Ivy-Ochs et al. 2006 and refs. therein). All of the analyzed basins are either within the limits of the LGM glaciation (Jäckli 1957) or in close proximity, and a

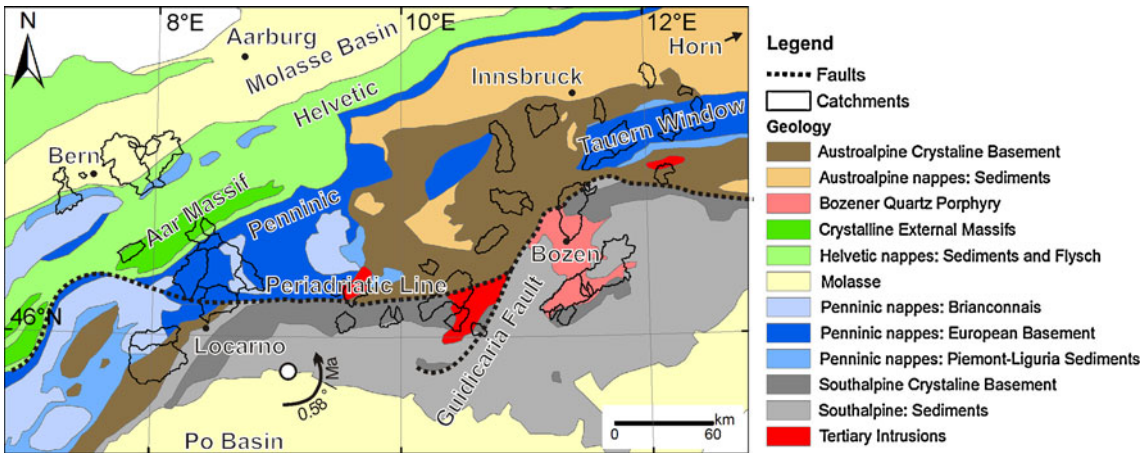

Fig. 1 Geologic setting of the Central and Eastern Alps

number of the catchments still retain active ice in their upper reaches. The Alpine glaciers deepened and widened the largest valleys, producing traps for post-glacial sediment (Hinderer 2001). Smaller tributary river systems throughout the Alps are stranded above the main valleys creating abundant knickzones and unstable slopes (Korup and Schlunegger 2007). The overall result is that hillslopes over much of the high Alpine relief are oversteepened and feed into shallow streams with prominent profile convexities and slot canyons near tributary junctions (Korup 2006; Robl et al. 2008a).

Modern precipitation rates in the Alps range from approximately 500–2,800 mm year^{-1} (Frei and Schär 1998). The highest values are typically located on the flanks of the orogen with dryer zones in its interior (Frei and Schär 1998). This effect is much more pronounced in the Eastern Alps, where the greater orogenic width causes a substantial zone of reduced precipitation. Specifically, the modern annual precipitation rate in the high Central Alps is 1,500 ± 400 versus 1,200 ± 300 mm year^{-1} for the Eastern Alps (Frei and Schär 1998). We use these climatic and morphometric values together with cosmogenic ^{10}Be-derived denudation rates to investigate the factors controlling surface morphology in the European Alps.

Methods

^{10}Be-derived basin-averaged denudation rates

In this study, we measured concentrations of cosmogenic nuclides in detrital quartz to determine basin-averaged denudation rates (von Blanckenburg 2005), which average over late Holocene timescales (0.5–3 ky). We measured concentrations of ^{10}Be in detrital quartz on 37 samples from 33 streams in the Eastern Alps of Northern Italy and Western Austria (Fig. 2a). Samples consisted of ~5 kg of sediment collected in the stream channels, on channel bars and on point bars. In all cases, the sediments sampled were part of the active stream channel. Samples were dried and sieved to 0.25–0.5- and 0.5–1-mm-size fractions for analysis. After sieving, magnetic grains were removed using a Frantz isodynamic magnetic analyzer. The non-magnetic fraction was then etched for 20 s in 24% HF, rinsed, dried, mixed with ~0.5 g 0.63-μm magnetite powder, and passed through the magnetic separator again in order to increase the quartz yield (Iacumin and Quercioli 1993). Samples were then treated with 5% HF until pure quartz remained. Approximately 0.2 mg ^{9}Be spike was added to ~50 g quartz. Dissolution and beryllium extraction methods were the same as those described in Norton et al. (2008, 2010b) and were performed at the University of Hannover. The pure beryllium was then evaporated and oxidized with $AgNO_3$ before being packed into targets for measurement at the AMS facility at ETH Zurich (Kubik and Christl 2010). ^{10}Be/^{9}Be ratios were measured relative to the standard S555 with a ^{10}Be/^{9}Be ratio of 95.5×10^{-12}, which is based on a half-life of 1.51 Ma for ^{10}Be. This half-life was used to derive the nominal ^{10}Be/^{9}Be ratio of the AMS standard only, in order to keep the results and interpretation consistent with our previous denudation rate data (Wittmann et al. 2007; Norton et al. 2008, 2010b) and with the production rates used (Schaller et al. 2002). Converting these resulting concentrations to the revised standard and half-life (Chmeleff et al. 2010) used at ETH Zürich since April 2010 would require increasing these reported rates by a factor of 1.096 (Kubik and Christl 2010). A laboratory blank of $1.2 \pm 0.4 \times 10^{-14}$ was subtracted from each sample and propagated into the error of the calculated denudation rates.

Denudation rates were determined from the ^{10}Be concentrations using the scaling laws of Dunai (2000) and the production rates and absorption laws compiled by Schaller

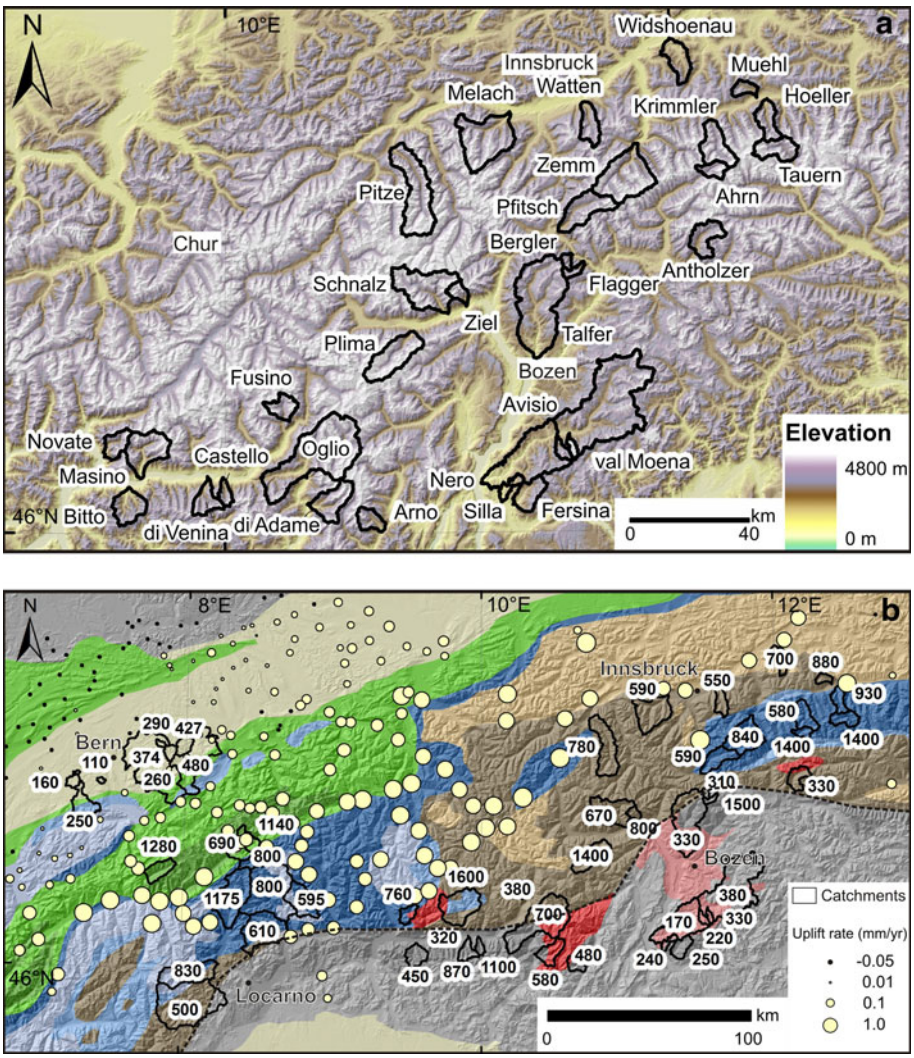

Fig. 2 **a** Eastern Alps drainage basins sampled for the new data shown here. **b** Central and Eastern European Alps basins showing denudation rates (mm ky^{-1}) and rock uplift rates (mm $year^{-1}$) and lithology. Rock uplift rates (*light circles*) are from Kahle et al. (1997), Schlatter et al. (2005) and preliminary data from the Eastern Alps from Ruess and Höggerl (2002). Studied basins in the Central Alps (Wittmann et al. 2007; Norton et al. 2008) and Eastern Alps are indicated by *black outlines*. Note that uplift rates are reported using mm $year^{-1}$, while denudation rates are reported in mm ky^{-1} in order to be consistent with the measurement integration time of each method

et al. (2002) for nucleons, as well as fast and stopped muons. We assumed a rock density of 2.7 g cm^{-3} and calculated our denudation rates with the revised ^{10}Be half-life of 1.39 Ma (Champagnac et al. 2009). Corrections for topographic and cover shielding were made; a correction for variations in the Earth's geomagnetic field was not necessary for this latitude. Topographic shielding factors (Table 1) were calculated from the 3D/2D surface area ratio for each basin based on the 90 m SRTM dataset (Norton and Vanacker 2009). We considered both snow and ice when calculating the shielding due to cover. Modern glacier outlines were taken from the World Glacier Inventory (National Snow and Ice Data Center 1999, updated 2009) and augmented with hand-digitized outlines from Landsat TM imagery where necessary. The ice-covered areas were assigned a production rate of 0 atoms g_{qtz}^{-1} $year^{-1}$ (e.g., complete attenuation). Snow-shielding factors were based on a snow-cover function (Norton et al. 2008) derived from Swiss snow-depth maps (Auer 2003). The applicability of the extrapolation of the Swiss altitude-dependent snow depth and duration function to the Eastern Alps was verified by comparing the snow-cover results to the monthly Modis/terra snow-cover dataset (Hall et al. 2006). The maximum snow-cover correction was <15%, with most values between 9 and 13% (Table 1).

In order to check the internal consistency of results, a duplicate of the 0.5–1-mm-size fraction of the Bergler sample was measured. Additionally, for 3 samples (Bergler, Flagger, and Höller, Fig. 2), both the 0.25–0.5 mm- and 0.5–1-mm-size fraction were analyzed. In each case, the measurements are within one standard deviation of one another, albeit with a large error on Höller (Table 1).

Lithologic and morphometric analysis

Bedrock lithologies for each basin were mapped from 1:500,000 scale geologic maps of Northern Italy (Compagnoni et al. 1983) and Austria (Geyer et al. 1923,

Table 1 Cosmogenic nuclide data for the Eastern Alps

Sample	Grain size (mm)	Altitude (m)	Longitude (dd)	Latitude (dd)	^{10}Be conc. (10^4 atoms g_{qtz}^{-1})	Topographic[a] shielding factor	Snow[a] shielding factor	Production rate[b] atoms (g_{qtz}^{-1} y^{-1})	Denudation rate[c] (mm ky^{-1})	Total error (mm ky^{-1})	Apparent age [d](year)
Ahrn	0.5–1	2,346	12.1730	47.0644	15.3 ± 2.7	0.87	0.85	36.0	1,230 ± 290	340	570 ± 130
Antholzer	0.5–1	1,941	12.1273	46.8596	49.1 ± 5.2	0.87	0.89	26.6	302 ± 50	65	2,380 ± 390
Arno	0.25–0.5	1,868	10.6241	46.0297	30.4 ± 2.4	0.87	0.89	25.4	469 ± 74	99	1,540 ± 240
Avisio	0.5–1	1,702	11.6603	46.3569	40.4 ± 6.3	0.98	0.91	22.3	359 ± 75	91	2,040 ± 430
Bergler	0.5–1	1,931	11.5090	46.7997	58.4 ± 6.1	0.84	0.89	26.7	246 ± 42	54	2,920 ± 500
Bergler 2	0.5–1	1,931	11.5090	46.7997	38.2 ± 4.6	0.84	0.89	26.7	376 ± 70	86	1,910 ± 360
Bergler 3	0.25–0.5	1,931	11.5090	46.7997	54.5 ± 4.2	0.84	0.89	26.7	264 ± 40	53	2,720 ± 420
Bitto	0.25–0.5	1,525	9.5687	46.0698	26.1 ± 3.2	0.86	0.92	19.2	436 ± 76	97	1,710 ± 300
Castello	0.25–0.5	1,773	9.9907	46.1094	12.1 ± 2.1	0.83	0.90	23.5	1,060 ± 230	270	690 ± 150
di Ada me	0.25–0.5	1,845	10.4612	46.0863	28.0 ± 3.0	0.84	0.90	24.5	480 ± 82	110	1,510 ± 260
di Venina	0.25–0.5	1,708	9.9068	46.0893	16.0 ± 3.9	0.82	0.91	22.2	760 ± 210	240	970 ± 270
Fersina	0.5–1	1,458	11.3241	46.1016	35.1 ± 5.5	0.91	0.93	18.0	325 ± 66	79	2,310 ± 470
Flagger	0.25–0.5	2,028	11.5353	46.7701	11.1 ± 2.2	0.84	0.88	28.6	1,370 ± 340	390	520 ± 130
Flagger 2	0.5–1	2,028	11.5353	46.7701	10.4 ± 1.9	0.84	0.88	28.6	1,470 ± 340	400	490 ± 110
Fusino	0.5–1	2,298	10.2435	46.3709	51.0 ± 3.5	0.86	0.86	35.0	356 ± 57	75	1,970 ± 320
Holler	0.25–0.5	1,964	12.4211	47.2050	22.7 ± 2.6	0.85	0.89	27.1	650 ± 110	140	1,110 ± 190
Holler 2	0.5–1	1,964	12.4211	47.2050	13.5 ± 5.3	0.85	0.89	27.1	1,090 ± 470	500	660 ± 280
Krimmler	0.25–0.5	2,283	12.1863	47.1335	33.2 ± 3.4	0.86	0.86	34.5	537 ± 95	120	1,310 ± 230
Lagorai	0.5–1	1,937	11.5167	46.2381	69.3 ± 7.0	0.87	0.89	26.5	214 ± 36	48	3,360 ± 570
Masino	0.25–0.5	1,973	9.6423	46.2411	47.5 ± 7.6	0.82	0.89	27.3	301 ± 63	75	2,380 ± 500
Melach	0.25–0.5	2,053	11.1531	47.1700	29.0 ± 2.2	0.87	0.88	29.1	548 ± 87	120	1,300 ± 210
Muhl	0.25–0.5	1,659	12.3205	47.3043	15.3 ± 2.2	0.91	0.91	21.4	850 ± 170	200	860 ± 170
Nero	0.5–1	1,431	11.5511	46.3087	39.7 ± 4.7	0.92	0.93	17.7	287 ± 50	64	2,620 ± 450
Novate	0.25–0.5	1,838	9.5134	46.2590	16.9 ± 2.2	0.75	0.90	24.4	710 ± 130	160	1,030 ± 190
Oglio	0.25–0.5	1,898	10.3930	46.2243	22.1 ± 2.5	0.88	0.89	25.7	660 ± 110	150	1,090 ± 190
Pfitsch	0.25–0.5	2,044	11.5939	46.9538	29.3 ± 4.0	0.86	0.88	28.7	530 ± 100	130	1,350 ± 260
Pitze	0.25–0.5	2,304	10.8355	47.0127	26.0 ± 3.5	0.84	0.86	35.0	680 ± 140	170	1,040 ± 210
Plime	0.25–0.5	2,181	10.7325	46.5199	15.3 ± 3.7	0.85	0.87	31.9	1,100 ± 300	340	650 ± 180
Schnalz	0.5–1	2,275	10.8789	46.7260	29.9 ± 3.6	0.84	0.86	34.3	580 ± 110	130	1,210 ± 220
Silla	0.5–1	954	11.2391	46.1247	36.6 ± 5.6	0.96	0.97	11.9	240 ± 47	57	3,310 ± 650
Talfer	0.5–1	1,689	11.3848	46.6758	41.1 ± 5.0	0.91	0.91	21.9	324 ± 57	72	2,260 ± 400
Tauern	0.25–0.5	2,302	12.4569	47.1196	14.9 ± 2.1	0.87	0.86	35.2	1,240 ± 240	300	570 ± 110
Val Moena	0.5–1	1,840	11.4730	46.2300	82.7 ± 6.3	0.87	0.90	24.6	168 ± 26	34	4,300 ± 660
Watten	0.5–1	1,929	11.6230	47.2091	29.3 ± 3.3	0.90	0.89	26.4	519 ± 90	110	1,390 ± 240

Table 1 continued

Sample	Grain size (mm)	Altitude (m)	Longitude (dd)	Latitude (dd)	^{10}Be conc. (10^4 atoms g_{qtz}^{-1})	Topographic[a] shielding factor	Snow[a] shielding factor	Production rate[b] atoms (g_{qtz}^{-1} y^{-1})	Denudation rate[c] (mm ky^{-1})	Total error (mm ky^{-1})	Apparent age [d](year)
Wildschoen	0.5–1	1,380	12.0251	47.3987	15.3 ± 2.9	0.92	0.94	17.1	730 ± 170	190	1,040 ± 240
Zemm	0.5–1	2,111	11.7756	47.0485	21.5 ± 2.7	0.81	0.87	30.3	710 ± 130	170	1,000 ± 190
Ziel	0.5–1	2,299	11.0255	46.7116	23.8 ± 3.3	0.84	0.85	35.3	750 ± 150	180	930 ± 190

[a] Topographic shielding was calculated from the SRTM database following Norton and Vanacker (2009) and snow-shielding corrections are based on annual Swiss snow data (Auer 2003)

[b] Production rates include topographic and snow shielding

[c] Denudation rate calculations based on the scaling laws of Dunai (2000) and production equations of Schaller et al. (2002) assuming cosmogenic steady state

[d] Apparent ages are calculated assuming cosmogenic steady state

1980) (Fig. 1). Non-quartz-bearing lithologies and areas upstream of hydroelectric dams were removed from the basin-contributing areas for the calculations of nuclide production rates, denudation rates, and morphometry. We additionally excluded the modern glaciers from the analysis so that the lower gradients of the ice did not affect the mean basin slopes or channel gradients. All topographic metrics were calculated from a 30-m DEM derived from topographic maps (de Ferranti 2005).

Hillslope gradients were averaged over each basin using a 3 × 3 cell sliding window. This slope map was also used to extract the gradient distributions for each bedrock class (Fig. 3). Channel steepness indices, k_{sn}, were calculated for each channel and normalized to a reference concavity, θ, equal to 0.45, which is used as a standard value for mountainous landscape such as the Alps (Korup 2006; Ouimet et al. 2009; Wobus et al. 2006). Both reference concavity and channel steepness index have been shown to be variable in both fluvial and glaciated environments (Brocklehurst and Whipple 2007; Whipple 2004; Wobus et al. 2006). Variation is therefore to be expected in measured k_{sn} values; however, the overall pattern of channel steepness in the Alps does not change significantly with different reference concavities (Norton et al. 2010a). Additionally, since both glaciated and non-glaciated environments are represented in individual rock-type categories, any variations should cancel out.

Rock uplift and climate analysis

The uplift rate of each basin was based on the centennial scale repeated leveling data of Kahle et al. (1997) and Schlatter et al. (2005) in Switzerland referenced to Aarburg. For the Austrian part of the Eastern Alps, we used the leveling-derived uplift rates of Ruess and Höggerl (2002), which are referenced to Horn, Austria. We interpret these data to represent rock uplift. This interpretation might appear confusing since Geodesists actually measure surface uplift. However, in this special case surface uplift equals rock uplift as there is no erosion of the geodetic measurement points over the timescale of leveling. Note that uncertainties, and the possibly preliminary nature, of Austrian uplift rate data do not allow them to be used in an absolute sense—however, they do provide us with an approximate indication of the magnitude and pattern of uplift. Despite using different reference stations, the two datasets compared well at the Swiss–Austrian border, with an average difference between the closest measurement pairs of 0.026 ± 0.211 mm $year^{-1}$. We therefore used these datasets without rescaling to new reference stations. Two approaches were used in determining the uplift rate for each basin. For basins in which one or more leveling point exists, the average uplift rate was used. Unfortunately, these uplift

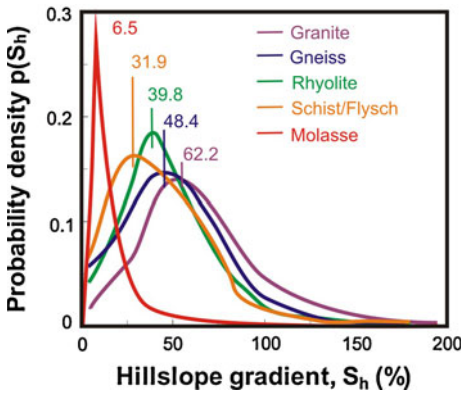

Fig. 3 Probability distribution of hillslopes for bedrock types. Korup (2008) showed that the probability of hillslope gradients, p(Sh), correlates with bedrock erodibility. Higher mean slope values indicate lower relative rock strength

datasets do not extend into northern Italy. If no uplift data existed within a drainage basin, it was assigned the value of the nearest leveling point. Due to the highly variable nature of rock uplift rates in the European Alps (Kahle et al. 1997; Schlatter et al. 2005), the uplift values from basins greater than ~25 km from the nearest leveling point should be treated with extreme caution. We used the raw data in favor of an interpolated surface because of the high variability and scarcity of data in the east. As no error assessment was available for the Austrian uplift data, we used the average measurement error of the Schlatter et al. (2005) dataset, 0.117 mm year^{-1}, for the entire uplift dataset. This measurement error was larger than the variability of uplift rates within the individual basins.

Finally, modern annual precipitation rates for the Alpine region (Frei and Schär 1998; Schwarb 2001) were obtained from monthly 1.25 min (~2 km) gridded PRISM datasets (Daly et al. 1994) spanning the time period from 1971 to 1990, supplied by Christoph Frei at the ETH Zürich (Frei and Schär 1998; Schwarb 2001). The mean annual values were calculated as the average of all values falling within the given basin and are reported with the standard deviation from this mean.

The new Eastern and Southern Alps data were then compared with data from the Central Alps (Norton et al. 2008; Wittmann et al. 2007). We did not use the entirety of these datasets, but have limited the data to those samples with representative basin size, the absence of excessive LGM deposits, and <10% recent glaciation. We recalculated the topographic metrics and mean rock uplift rates for the Central Alpine basins (Norton et al. 2008; Wittmann et al. 2007) using the 30-m resolution DEM for consistency, following the procedures above. Note that we report all rates in units that relate to the integration time of their measurements. Hence, cosmogenic nuclide-based denudation rates are reported as mm ky^{-1}, and both geodesy-based uplift and convergence rates in mm year^{-1}.

Results

^{10}Be-derived basin-averaged denudation rates from the Eastern Alps range from 170 to 1,400 mm ky^{-1} (Table 1; Fig. 2b) and vary considerably between lithologies (Fig. 4). Rates from the crystalline units north of the Periadriatic Lineament average 700 ± 310 mm ky^{-1}, while the surrounding nappes are eroding at an average of 480 ± 280 mm ky^{-1}. The average denudation rate of the Eastern Alpine crystalline units north of the Periadriatic Lineament is statistically indistinguishable from that of the similar lithologies in the Central Alps (800 ± 300 mm ky^{-1}). Mean basin

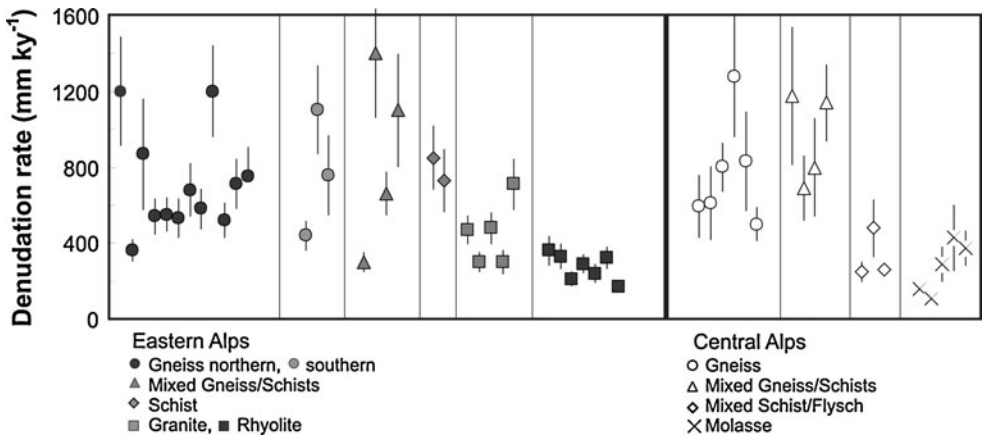

Fig. 4 Denudation rates in the Eastern Alps (this study) and Central Alps (Wittmann et al. 2007; Norton et al. 2008) sorted by lithology. Note that rhyolite sites erode at a significantly lower rate than other lithologies of the Eastern Alps, $t(31) = 6.53$, $p < 0.001$. Granite sites erode at a significantly lower rate than other lithologies of the Eastern Alps, $t(11) = 1.85$, $p = 0.045$, and catchments underlain by Granite and Rhyolite lithologies erode at a significantly lower rate than other lithologies of the Eastern Alps, $t(31) = 5.23$, $p < 0.001$

Table 2 Geologic and topographic parameters

Name	Bedrock[a]	Area (km^2)	Mean elevation[b] (m)	Mean slope[b] (%)	Glacial cover[c] (%)	Channel Steepness[d]	Rock uplift rate[e] (mm $year^{-1}$)	Distance[f] (km)
Ahrn	Gneiss North	36	2,346	58.9	6	160	*1.24*	29
Antholzer	Mixed Granite/Gness	79	1,941	57.9	1	174	*0.34*	*41*
Arno	Granite	47	1,868	57.9	0	201	*1.18*	*73*
Avisio	Rhyolite	565	1,702	46.2	0	156	*1.64*	*61*
Bergler	Granite	14	1,931	64.6	0	229	1.64	24
Bitto	Gneiss South	86	1,525	59.4	0	216	1.06	24
Castello	Gneiss South	26	1,773	68.9	0	250	105	*34*
di Adame	Granite	98	1,845	64.9	4	280	*1.15*	*61*
di Venina	Gneiss South	60	1,708	69.5	1	303	*1.05*	*30*
Fersina	Rhyolite	71	1,458	47.2	0	170	*1.64*	*99*
Flagger	Mixed Granite/Gness	18	2,028	65.7	0	166	*1.64*	*28*
Fusino	Gneiss North	53	2,298	60.1	2	197	*1.18*	*28*
Hoeller	Gneiss North	64	1,964	63.7	0	198	1.24	3
Krimmler	Gneiss North	100	2,283	61.2	8	183	1.24	23
Lagorai	Rhyolite	15	1,937	57.1	0	164	164	85
Masino	Granite	133	1,973	71.1	3	277	1.06	5
Melach	Gneiss North	220	2,053	57.9	3	190	0.76	3
Muehl	Schist	29	1,659	46.6	0	144	1.24	8
Nero	Rhyolite	841	1,431	45.4	0	173	164	67
Novate	Granite	54	1,838	85.4	0	251	1.06	4
Oglio	Mixed Granite/Gness	411	1,898	55.9	1	194	*1.18*	*40*
Pfitsch	Gneiss North	119	2,044	61.1	6	164	1.64	8
Pitze	Gneiss North	225	2,304	66.2	11	226	0.99	9
Plima	Mixed Granite/Gness	143	2,181	61.3	6	278	178	*38*
Schnalz	Gneiss North	199	2,275	64.5	2	263	177	*25*
Silla	Rhyolite	25	954	31.2	0	81	178	*98*
Talfer	Rhyolite	375	1,689	46.6	0	156	7.64	*25*
Tauern	Gneiss North	77	2,302	57.5	12	185	1.24	14
val Moena	Rhyolite	22	1,840	56.7	0	160	7.64	*86*
Watten	Gneiss North	63	1,929	49.6	0	184	0.86	15
Widshoenau	Schist	76	1,380	44.0	0	119	0.90	4
Zemm	Gneiss North	210	2,111	72.2	12	258	1.64	12
Ziel	Gneiss North	30	2,299	64.6	0	291	*1.77*	*43*

[a] Bedrock lithology was taken from the geologic maps of Northern Italy (Compagnoni et al. 1983) and Austria (Geyer et al. 1923)

[b] Topographic metrics were derived using the 30 m DEM

[c] Channel steepness was calculated using a reference concavity of 0.45 (Wobus et al. 2005)

[d] Glacial cover for each basin was determined using the World Glacier Inventory (National Snow and Ice Data Center 1999, updated 2009)

[e] Rock uplift rates (Ruess and Höggerl 2002) are the average of all measured values within a catchment, or the value of the closest measured value. Italics indicate more than 25 km spacing between the basin and uplift measurements

[f] Distance between the drainage basin and the nearest measured rock uplift rate

elevations are between 940 m and 2,340 m asl. Channel steepnesses and mean basin hillslope gradients vary from 80 to 300 $m^{0.9}$ and 12–38°, respectively (Table 2). Relative rock uplift rates of 0.34–1.71 mm $year^{-1}$ have been measured within the studied basins (Kahle et al. 1997; Ruess and Höggerl 2002; Schlatter et al. 2005).

Denudation rates in the Eastern Alps differ considerably across lithologic boundaries (Fig. 4). This is, however, also the case for the Central Alpine data when separated by lithology (Fig. 4). The lowest average rates are recorded from Tertiary igneous rocks at $\sim 450 \pm 30$ mm ky^{-1} (granitic intrusions of the Bergell, Adamello, and

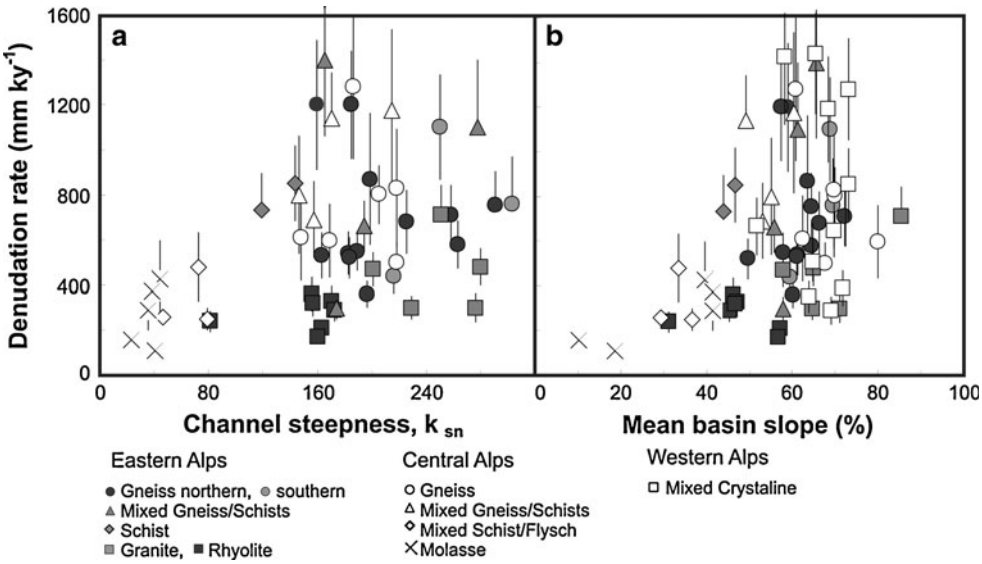

Fig. 5 Topographic metrics for the Central (Wittmann et al. 2007) and Eastern Alps. Denudation rate (mm ky^{-1}) plotted against **a** channel steepness index, k_{sn}, and **b** mean basin slope, including the Western Alps (Delunel et al. 2010)

Rieserferner) and Permian rhyolitic extrusives at $\sim$274 $\pm$ 70 mm ky^{-1} (Bozener Quartz Porphyry) and the sedimentary rocks of the Molasse at $\sim$330 $\pm$ 130 mm ky^{-1}. The highest average rates are from mixed lithologies and pre-Alpine crystalline basement rocks at 810 $\pm$ 70 mm ky^{-1} (Fig. 4).

One of the most striking results, however, is that the correlations between denudation rate and basin morphometry, which are apparent in the Central Alps of Switzerland (Wittmann et al. 2007) do not exist in the Eastern or Western Alps (Delunel et al. 2010) (Fig. 5). Denudation rates show a wide scatter with both channel steepness (Fig. 5a) and mean basin slope (Fig. 5b). Interestingly, clear relationships between topographic metrics and denudation rates with precipitation rates (Fig. 6) are likewise non-existent. Channel steepness indices and mean basin slopes show no systematic variation with precipitation rates (Fig. 6a, b), and there is a wide range of denudation rates across the precipitation gradient (Fig. 6c).

Rock uplift rates are also uncorrelated with denudation rates for the Eastern Alps (Fig. 7), which thus contrasts with the Central Alps where a correlation in the data exists (Wittmann et al. 2007). The relationship between channel steepness and rock uplift rates for the Eastern Alps generally follows the trend of the Central Alpine data, but is likewise not statistically significant. However, even taking into consideration the low density and possibly reduced precision of Eastern Alps leveling data, denudation rates in the Eastern Alps are generally lower than rock uplift rates (Fig. 7a).

It is also worth noting that the major Alpine tectonic boundaries do not seem to have a major influence on denudation rates. In particular, denudation rates on the northern and southern side of the Periadriatic Lineament in the Adda Valley (Fig. 2b) are similar, also rates in the Penninic Tauern Window are similar to those of the overthrusted Ötztal basement and to those of catchments within the overthrusted Paleozoic nappes north of the Tauern Window. This suggests that these boundaries have been inactive for at least the millennial timescale of our measurements or have had no impact on the geomorphic evolution of the units they separate. There is, however, one noteworthy exception. Denudation rates of 530–1,200 mm ky^{-1} in the Tauern Window decrease to much lower rates toward the south, averaging $\sim$300 mm ky^{-1} (Figs. 2b, 4). A purely tectonic cause for this gradient cannot however be inferred as this is also the site of a change in dominant bedrock lithology from gneiss to granite and rhyolite (see below).

Discussion

Lithologic controls

Denudation rates vary considerably with rock type (Fig. 4). The relationship is not equally strong for all rock types, with the most homogeneous rates coming from both weaker (Molasse and schist) and stronger (rhyolite and granite) lithologies. The highest variability is associated with gneisses and basins with mixed lithologies (Fig. 4). Kühni and Pfiffner (2001) presented relative rock erodibility classes that were corroborated by field measurements of rock mass strength by Korup and Schlunegger (2009) for the rocks of the eastern Swiss Alps. The most erodible rocks are the Molasse and Flysch units followed by schists, the carbonates of the nappe stacks (Helvetics, Penninics, Eastern Alpine nappes, South Alpine units), pre-Mesozoic basement paragneisses, and finally the Tertiary

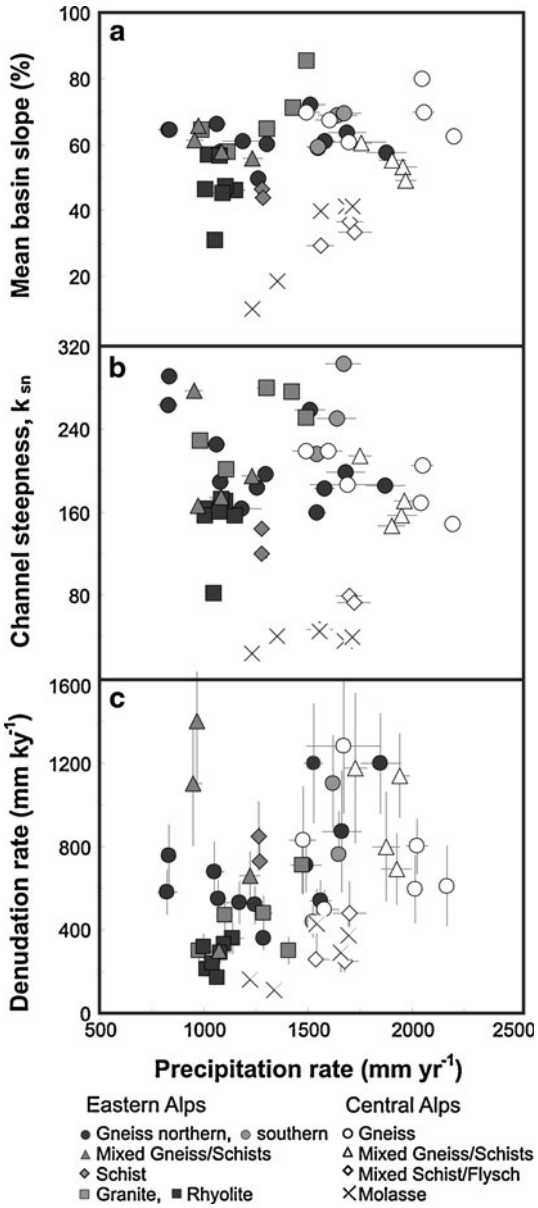

Fig. 6 Precipitation rate (mm year^{-1}) plotted against **a** channel steepness index, k_{sn}, and **b** mean basin slope. **c** Denudation rate (mm ky^{-1}) plotted against mean annual precipitation rate (mm year^{-1}). *Error bars* on precipitation rates show the 1-sigma variation of annual precipitation rate within each catchments and therefore record likely variability and not measurement uncertainty

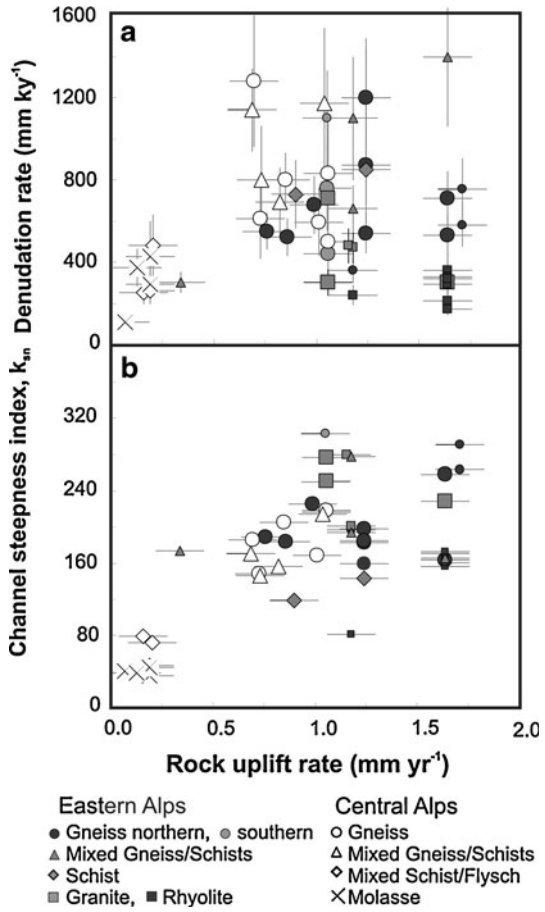

Fig. 7 **a** Denudation rate (mm ky^{-1}) and **b** channel steepness index, k_{sn}, plotted against relative rock uplift rate (mm year^{-1}). Due to the paucity of uplift rate data in the Eastern Alps, which in any case represents only a first approximation to rock uplift, basins for which the nearest uplift measurement was farther than 25 km away are shown by *half-sized symbols*

intrusives. While the Bozener Quartz Porphyry does not crop out in the Swiss Alps and was therefore not categorized by Kühni and Pfiffner (2001), we suggest that it should also exhibit low to medium erodibilities, on the order of the schists to granitoids based on the hillslope probability distribution (Fig. 3). Korup (2008) suggested that the slope distribution for each lithologic unit is a function of the relative resistance of the rock to erosion.

Some of this correlation between rock type and denudation rate might be caused by factors other than rock composition per se. For instance, Molnar et al. (2007) suggested that fracturing is also an important control on rock strength and resistance to erosion. In the Alps, the shallow parts of the Tertiary granitic intrusions did not experience the same deformation as the deeply exhumed crystalline basement rocks; they are fractured in a different way and therefore potentially less erodible. These rocks often form the high-altitude core of mountain belts (Molnar et al. 2007). Similar processes might be at work in the Alps, where low-grade metamorphic schists have high denudation rates, whereas granite and rhyolite (the latter having been extruded at the surface and exposed since the Permian) feature low erodibility. Some of this lithologic control might also be caused by the dip of sedimentary and folded metamorphic foliations, which also controls the way catchments drain and erode (Schwab et al. 2009). In the high Alps, variably fractured bedrock with strong metamorphic fabrics, such as gneisses and schists, are presumed to have the largest variability in erodibility, which might

explain the large scatter of the denudation rate data in these basins (Fig. 4).

It is not, however, the case that the lowest erodibilities are always associated with low denudation rates and vise versa. If this were the case, then the lowest rates would be measured in the high Alps in the crystalline lithologies, and the highest in the foreland basins in Molasse and flysch sediments. Lithology has a clear impact on the distribution of slope gradients in the Alps (Fig. 3). The more resistant lithologies display higher hillslope modes irrespective of their location in the range (e.g., Kühni and Pfiffner 2001). This is also apparent in the analyzed catchments. Basins underlain by the Molasse, schist or flysch have lower channel steepness indices and mean slope gradients than those underlain by granites and gneisses (Table 2; Fig. 6a, b). In these hillslopes with low soil cover, bedrock strength determines the threshold angle for hillslopes. Resistant bedrock such as the granites of the Bergell and Adamello intrusions and the basement gneisses are capable of sustaining very steep slopes, whereas the more erodible lithologies are associated with lower average slopes, irrespective of erosion, as is the case in the high Central Alps when analyzed separately (Wittmann et al. 2007). The opposite end of the spectrum can be seen in the Molasse Basin, where correlation coefficients between denudation rates, basin morphometrics, and rock uplift rates are invariably high (Wittmann et al. 2007). The good correlations in the Molasse Basin can be explained by the prevailing hillslope-sediment transport regime. The hillslopes of the Molasse are soil-mantled (Schlunegger and Schneider 2005; Norton et al. 2008), and erosion is controlled by sediment transport and thus by hillslope and channel gradients instead of rock strength alone (e.g., Montgomery 2001).

Driving forces of denudation and uplift

The pattern of rock uplift in the Alps has been explained alternatively as a response to removal of a subducted slab (Lippitsch et al. 2003), ongoing convergence (Persaud and Pfiffner 2004), glacio-isostatic rebound (Gudmundsson 1994) or isostatic compensation to erosion (Champagnac et al. 2007). As stated earlier and discussed in detail by Wittmann et al. (2007), rock uplift rates in the Central Alps have been suggested to correlate with denudation rates and basin morphometric indices. These relationships are also seen in orogens worldwide (Binnie et al. 2007; DiBiase et al. 2010; Ouimet et al. 2009; Safran et al. 2005). Champagnac et al. (2009) modeled this uplift pattern for the Central Alps as an isostatic response to denudation. Norton et al. (2010a) suggested glacial perturbation as a potential mechanism to drive these high rates. In this way, the thickest and most erosive glaciers during the LGM and earlier glaciations conditioned valleys and hillslopes for high rates of Holocene erosion and consequently rock uplift via isostatic compensation.

The correlations in the Central Alps between basin morphology, denudation rate, and uplift rate do not exist for the Eastern Alps (Figs. 6, 7). Bearing in mind that the rock uplift data in the Eastern Alps is preliminary, we now assess the links between denudation, basin morphometry, precipitation, and rock uplift modified by lithology as potential causes of the data variability. We specifically address the twin observations that there is no correlation of climatic and morphometric parameters with denudation rates in the Eastern Alps and that rock uplift rates are, on average, higher than denudation rates. Interestingly, although the European Moho depth beneath the Central and Eastern Alps is similar, the mean elevation of the Eastern Alps is lower than the Central Alps (Robl et al. 2008a). We discuss the expression of these geomorphic and climatic features within the context of the stages of orogenic evolution outlined in the introduction, and also as a result of geomorphic inheritance introduced by climate change.

Geomorphic expressions of the Eastern Alps in pure convergence

In the case of a convergent orogen in topographic steady state, the rock uplift rate U_R equals the denudation rate D, which is in turn equal to the ratio of the mass flux into the range divided by its width W (Whipple 2009):

$$D = U_R = \frac{V * Z}{W} \quad (1)$$

where V is the convergence rate across the orogen and Z is the thickness of the accreting crust. Assuming a thickness of 30 km for the accreting European crust, a convergence rate of 2 mm year^{-1} and an orogenic width of 50 km in pre-Miocene time when shortening was focused in the Tauern Window (Rosenberg and Berger 2009), we calculate a maximum rock uplift rate of 1.2 mm year^{-1} for the Eastern Alps. If we assume instead that the flux is accommodated over the entire width of the Eastern Alpine range ($\sim$250 km), then we calculate a minimum uplift rate of 0.24 mm year^{-1}. Although we are unable to assess the likelihood of either end-member scenario, they do suggest that modern rock uplift rates are on the order of what would be expected if they were entirely due to convergence. We note, however, that if the entire convergent flux were accommodated within the Tauern Window, uplift would not occur elsewhere, which contradicts the measured rock uplift rates (Ruess and Höggerl 2002). Therefore, the lower range of estimates is more likely, in which case the average measured rock uplift rates in the mountainous Eastern Alps are higher than can be explained by convergent flux alone.

Rock uplift solely by isostatic compensation of the eroding Eastern Alps

A strong case can be made for rock uplift only by isostatic compensation of the eroding Central Alps (Wittmann et al. 2007; Champagnac et al. 2009). In a purely erosion-controlled system (with no collisional flux), one would expect a systematic relationship between denudation rates and climate parameters. Indeed, mean basin slopes in the Central Alps do weakly correlate with precipitation rate (Fig. 6a; $R^2 = 0.59$). Correlations of precipitation rate with channel steepnesses (Fig. 6b; $R^2 = 0.42$) and denudation rates (Fig. 6c; $R^2 = 0.39$) are also apparent. In the Eastern Alps, there are no such correlations between basin slope, channel steepness, and denudation rate (Fig. 6; $R^2 = 0.06$, 0.01, and 0.13, respectively). This implies that modern climate is not the major factor controlling erosional processes in the Eastern Alps. However, Alpine surface processes are probably still responding to perturbations by the LGM and earlier glaciations (e.g., Norton et al. 2010a).

A second line of evidence supporting isostatically driven uplift of the Central and not of the Eastern Alps is the relationship between channel steepness and denudation rate. Ouimet et al. (2009) showed that the channel steepness index, k_{sn}, continues to correlate with denudation rate beyond the range for which hillslope gradients correlate. The channel steepness index is sensitive to changes in lithology (Safran et al. 2005), glacial perturbation (Brocklehurst and Whipple 2002) and rock uplift rate (Snyder et al. 2000, 2003). Channel steepness indices in the Central Alps do increase with increasing rock uplift rates in the basins studied (Fig. 7b; $R^2 = 0.93$), as expected in basins where there is a close link between uplift and erosion. In contrast, the data from the Eastern Alps are highly variable (Fig. 7b; $R^2 < 0.01$), suggesting that uplift has not left an imprint on channel gradients. The same trend exists between denudation and uplift. The Central Alps data correlate well (Fig. 7a; $R^2 = 0.71$), whereas the Eastern Alps display a wide scatter in denudation rates versus rock uplift rates (Fig. 7a; $R^2 = 0.09$). Hence, in contrast to the Central Alps, the lack of correlation in the Eastern Alps supports two conclusions: (1) rock uplift is not a driving force for denudation in the Eastern Alps; (2) rock uplift cannot be interpreted as a response to erosional unloading in a non-collisional orogen. In other words, the erosion of the Eastern Alps cannot be interpreted as being in steady state with either tectonic mass flux or erosion-driven uplift.

Surface uplift in the Eastern Alps by combined deformation and isostatic compensation

Stüwe and Barr (1998) showed that the combination of convergence and isostatic compensation leads to higher rates of rock uplift than either process alone. This case can be illustrated by the clear distinction between the denudation styles in the Central and Eastern Alps. In the Central Alps, convergence rates are non-measurable and isostatic response ensures that surface erosion results in rock uplift. Therefore, strong correlations exist between environmental, topographic, and rock velocity parameters. These strong correlations are not evident in the Eastern Alps. Additionally, denudation rates clearly plot above the 1:1 line of denudation rate to rock uplift rate (Fig. 8), suggesting that the Eastern Alps are undergoing active surface uplift. Even though this inference is strongly dependent on the choice of the reference station for the rock uplift rates, the Austrian reference station at Horn is sufficiently distant from the center of the belt for it to represent a meaningful base level for the Eastern Alps. Indeed, evidence for a recent increase (<5 My) in rock uplift rates was reported from the easternmost margin of the Eastern Alps where an increase in the rates of valley incision was interpreted to reflect consecutive uplift and river capture (Wagner et al. 2010). Such wide-spread surface uplift cannot occur through purely isostatic mechanisms. Therefore, a tectonic driver needs to be invoked (Wagner et al. 2010). We can only speculate as to whether this driver is continued convergence (Grenerczy et al. 2005), glacio-isostatic rebound (Gudmundsson 1994), removal of a deep lithospheric root whose downward force previously kept the belt in a state of overcompensation (e.g., Lyon-Caen and Molnar 1989) or a change in subduction polarity beneath the study area (Schmid et al. 2004). A change in subduction polarity, for example, would have been preceded by slab breakoff, which would induce lithospheric uplift both by eliminating dynamic subsidence

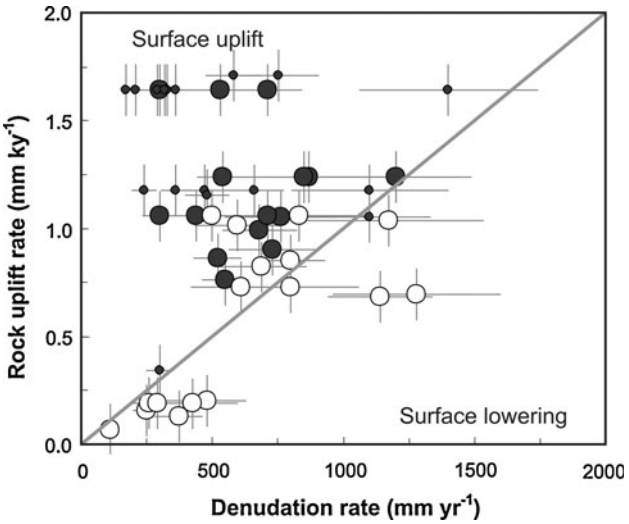

Fig. 8 Inversion of Fig. 7b. The data from the Eastern Alps consistently plot above the 1:1 line, indicating surface uplift of these basins with respect to the Alpine Foreland

as subduction stopped and by removing the load of the slab (Davies and von Blanckenburg 1995). Depending on the depth of breakoff, the resulting uplift could have amounted to 2–6 km (Buiter et al. 2002).

Differential geomorphic inheritance from LGM glacial erosion

Finally, transient surface processes may also lead to the observed distribution of denudation rates in the Eastern and Southern Alps. Glacial sculpting and oversteepening of valleys during the time of the LGM has been shown to result in increased Holocene denudation rates for such valleys in the Central Alps, while valleys experiencing only Holocene fluvial dissection denude at low rates (Norton et al. 2010b). Furthermore, Norton et al. (2010a) showed that the cumulative effect of LGM glaciation in the Central Alps is the creation of steep, disequilibrium landscapes (e.g., Brocklehurst and Whipple 2002) in which post-glacial fluvial erosion rates are focused through enhanced stream power. The reverse argumentation can also be used to explain the more distributed pattern of denudation rates in the Eastern Alps, with less intense glacial preconditioning during LGM due to less pervasive glacial erosion. Pleistocene glaciation of the Central Alps was focused on the main topographic divide (Bini et al. 2009), whereas the main centers of glaciation in the Eastern Alps were spread over a wider area (e.g., Adamello, Bergel, Ötztal, Tauern Window). This hypothesis is also partially supported by both modern and paleoclimatological data. Modern precipitation rates are high throughout the Central Alps, but are ~50% lower in most of the Eastern Alps, with the major east–west valleys being the driest locations (Frei and Schär 1998). The same situation occurred during glacial periods. Kerschner and Ivy-Ochs (2008) showed that the ELA of Alpine glaciers during the Younger Dryas was up to 300 m higher in the central Alpine valleys than on the fringes, indicating either higher temperatures or lower precipitation rates. Additionally, Florineth and Schlüchter (1998) argued for a southerly air circulation pattern during the LGM, leading to low ELAs south of the Alpine range. However, the interior valleys of the Eastern Alps during this climate period would still remain dry due to orographic rainout at the Alpine margin. So even though general concepts of glacial erosion predict higher mean elevations for higher ELAs, due to limits on sustainable relief (Whipple et al. 1999; Brocklehurst and Whipple 2002), the combination of lower average elevation and a dryer interior during LGM times resulted in smaller accumulation areas and therefore generally smaller glaciers in the core of the Eastern Alps than in the Central Alps. This reduced glacial pre-conditioning, added to the wide spatial distribution of glaciers in the Eastern Alps, and potentially supports less focused and lower fluvial Holocene denudation rates.

Conclusions

The combination of denudation rate measurements with topographic, climatic, and uplift parameters allows one to distinguish tectonic and geomorphic controls on erosion in the European Alps. Four main conclusions can be drawn from these data: (1) correlations between denudation rates and all morphometric parameters measured here are good in the Central Alps and non-existent in the Eastern Alps, where denudation rates as a whole are widely variable and loosely related to lithology; (2) average denudation rates are similar in the Eastern and Central Alps: (3) apparent rock uplift rates are higher than most denudation rates in the Eastern Alps, such that surface uplift appears to be taking place today; and (4) unlike the situation during the Oligocene and Miocene, spatial patterns of denudation do not follow tectonic boundaries in the Eastern and Southern Alps.

The large scatter in denudation rates within individual lithologic groups suggests that there is considerable variation in resistance to erosion for each bedrock class, which might be explained by differences in tectonic pre-conditioning through fracturing and the dip of foliation. A better understanding of the effects of differences in fracture spacing and orientation, bedrock mineralogy, shear directions, and other bedrock properties on hillslope-scale denudation rates would help to further constrain these trends.

The good correlations between denudation rate and uplift rate in the Central Alps are interpreted to indicate a state of isostatic compensation in which denudation controls rock uplift. The lack of such correlations in the Eastern Alps shows that denudation is not the only control of rock uplift. There, a tectonic force associated with slow counterclockwise rotation and convergence of Adria with respect to Europe (Grenerczy et al. 2005) may be acting to provide additional uplift. Such a driver is apparent only in the Eastern Alps, also because the denudation is less focused than in the Central Alps. In the Central Alps, large, centralized glaciers carved deep valleys and created an oversteepened and highly erodible landscape. In the Eastern Alps, the LGM glaciers were more widely distributed, resulting in less glacial overprinting and hence less acceleration of Holocene erosion. The combined effect of multiple uplift forces and weak erosional forces is that rock uplift rates in the Eastern Alps exceed denudation rates. This supports the inference that surface uplift and orogen-wide relief growth is occurring in the Eastern Alps.

However, this possibility is contingent on greater amounts of more accurate rock uplift data for the Eastern and Southern Alps.

Finally, we observe that the area of highest erosion rates in the present Eastern Alps is not delimited by tectonic boundaries. Rather, it occupies large parts of both the Tauern window and the nappes of the overriding orogenic lid, as well as, south of the Periadriatic lineament for some lithologies. Therefore, the spatial distribution of denudation switched from the narrow belt of the Tauern Window in late Tertiary time to the entire formerly glaciated Eastern Alps at some stage within the Quaternary.

Acknowledgments We are grateful to the reviews by Kurt Stüwe and Jean-Daniel Champagnac, the detailed remarks and excellent editorial handling of Mark Handy, and comments from Nicolas Legrain and Jean Dixon. We acknowledge financial support to F.v.B. by the European Science Foundation Project "TopoAlps" and by DFG grant BL562-2. As an undergraduate, F.v.B. was fascinated and inspired to study Alpine Geology by Rudolf Trümpy's lectures and field courses.

References

Auer M (2003) Regionalisierung von Schneeparametern—Eine Methode zur Darstellung von Schneeparametern im Relief. Universität Bern, 97 pp

Battaglia M, Murray MH, Serpelloni E, Bürgmann R (2004) The Adriatic region: an independent microplate within the Africa-Eurasia collision zone. Geophys Res Lett 31:L09650

Bernet M, Brandon M, Garver J, Balestieri ML, Ventura B, Zattin M (2009) Exhuming the Alps through time: clues from detrital zircon fission-track thermochronology. Basin Res 21:781–798

Bini A, Buoncristani J-F, Couterrand S, Ellwanger D, Felber M, Florineth D, Graf HR, Keller O, Kelly M, Schlüchter C, Schoeneich P (2009) Switzerland during the last maximal: Swisstopo, scale 1:500000, Wabern

Binnie SA, Phillips WM, Summerfield MA, Fifield LK (2007) Tectonic uplift, threshold hillslopes, and denudation rates in a developing mountain range. Geology 35:743

Brocklehurst SH, Whipple KX (2002) Glacial erosion and relief production in the Eastern Sierra Nevada, California. Geomorphology 42:1–24

Brocklehurst SH, Whipple KX (2007) Response of glacial landscapes to spatial variations in rock uplift rate. J Geophys Res 112:F02035

Brückl E, Behm M, Decker K, Grad M, Guterch A, Keller GR, Thybo H (2010) Crustal structure and active tectonics in the Eastern Alps. Tectonics 29. doi:10.1029/2009TC002491

Buiter JH, Govers R, Wortel MJR (2002) Two-dimensional simulations of surface deformation caused by slab detachment. Tectonophysics 354:195–210

Calais E, Nocquet J-M, Jouanne F, Tardy M (2002) Current strain regime in the Western Alps from continuous Global Positioning System measurements, 1996–2001. Geology 30:651–654

Cederbom CE, Sinclair HD, Schlunegger F, Rahn MK (2004) Climate-induced rebound and exhumation of the European Alps. Geology 32:709–712

Champagnac J, Molnar P, Anderson R, Sue C, Delacou B (2007) Quaternary erosion-induced isostatic rebound in the western Alps. Geology 35:195–198

Champagnac J-D, Schlunegger F, Norton KP, von Blanckenburg F, Abbühl LM, Schwab M (2009) Erosion-driven uplift of the modern Central Alps. Tectonophysics 474:236–249

Chmeleff J, von Blanckenburg F, Kossert K, Jacob D (2010) Determination of the ^{10}Be half-life by multicollector ICP-MS and liquid scintillation counting. Nucl Instrum Methods Phys Res B 268:192–199

Compagnoni B, Damiani A, Valletta M, Finetti I, Cirese E, Pannuti S, Sorrentino F, Rigano C (1983) Carta Geologica D'Italia: Servizio Geologico D'Italia, scale 1:500000. Rome

Daly C, Neilson RP, Phillips DL (1994) A statistical-topographic model for mapping climatological precipitation over mountainous terrain. J Appl Meteorol 33:140–158

Davies JH, von Blanckenburg F (1995) Slab breakoff: a model of lithosphere detachment and its test in the magmatism and deformation of collisional orogens. Earth Planet Sci Lett 129:85–102

de Ferranti J (2005) 1″ resolution digital elevation data for the European Alps. http://www.viewfinderpanoramas.org\dem3.html

Delunel R, van der Beek PA, Carcaillet J, Bourlès DL, Valla PG (2010) Frost-cracking control on catchment denudation rates: insights from in situ produced ^{10}Be concentrations in stream sediments (Ecrins-Pelvoux massif, French Western Alps). Earth Planet Sci Lett 293:72–83. doi:10.1016/j.epsl.2010.02.020

Dewey JF (1988) Extensional collapse of orogens. Tectonics 7:1123–1139

DiBiase RA, Whipple KX, Heimsath AM, Ouiment WB (2010) Landscape form and millennial erosion rates in the San Gabriel Mountains, CA. Earth Planet Sci Lett 289:134–144

Dunai TJ (2000) Scaling factors for production rates of in situ produced cosmogenic nuclides: a critical reevaluation. Earth Planet Sci Lett 176:157–169

England P, Molnar P (1990) Surface uplift, uplift of rocks, and exhumation of rocks. Geology 18:1173–1177

Florineth D, Schlüchter C (1998) Reconstructing the last glacial maximum (LGM) ice surface geometry and flowlines in the Central Swiss Alps. Eclogae Geologicae Helvetica 91:391–407

Frei C, Schär C (1998) A precipitation climatology of the Alps from high-resolution rain-gauge observations. Int J Climatol 18:873–890

Geyer G, Hammer W, Beck H, Götzinger G, Spengler E, Vetters H, Waagen L, Winkler A (1923, 1980) Geologische Karte der Republik: Geologische Bundesanstalt, scale 1:500000. Wien

Grenerczy G, Sella G, Stein S, Kenyeres A (2005) Tectonic implications of the GPS velocity field in the northern Adriatic region. Geophys Res Lett 32:L16311. doi:10.1029/2005GL022947

Gudmundsson GH (1994) An order-of-magnitude estimate of the current uplift-rates in Switzerland caused by the Würm Alpine deglaciation. Eclogae Geologicae Helvetiae 87:545–557

Hall DK, Riggs GA, Salomonson VV (2006) MODIS snow and sea ice products. In: Qu J (ed) Earth science satellite remote sensing—volume 1: science and instruments. Springer, Berlin

Handy MR, Babist J, Rosenberg CL, Wagner R, Konrad M (2005) Decoupling and its relation to strain partitioning in continental lithosphere—insight from the periadriatic fault system (European Alps). In: Gapais D, Brun JP, Cobbold PR (eds) Deformation mechanisms, rheology and tectonics, vol 243. Geological Society Special Publications, London, pp 249–276

Handy MR, Schmid S, Bousquet R, Kissling E, Bernoulli D (2010) Reconciling plate-tectonic reconstructions of Alpine Tethys with the geological-geophysical record of spreading and subduction in the Alps. Earth Sci Rev. doi:10.1016/j.earscirev.2010.06.002

Hinderer M (2001) Late quaternary denudation of the Alps, valley and lake fillings and modern river loads. Geodinamica Acta 14:231–263

Iacumin P, Quercioli C (1993) A new technique for quantitative separation of quartz from feldspars. Eur J Mineral 5:677–678

Ivy-Ochs S, Kerschner H, Reuther A, Maisch M, Sailer R, Schaefer J, Kubik PW, Synal H-A, Schlüchter C (2006) The timing of glacier advances in the northern European Alps based on surface exposure dating with cosmogenic ^{10}Be, ^{26}Al, ^{36}Cl, and ^{21}Ne. Geol Soc Am Spec Pap 415:43–60

Jäckli H (1957) Gegenwartsgeologie des Bündnerischen Rheingebietes, vol 36. Beitrage zur Geologie der Schweiz, Zurich, p 136

Kahle HG, Geiger A, Buerki B, Gubler E, Marti U, Wirth B, Rothacher M, Gurtner W, Beutler G, Bauersima I, and Pfiffner OA (1997) Recent crustal movements, geoid and density distribution: contribution from integrated satellite and terrestrial measurements. In: Pfiffner OA (eds) Results of the National Research Program 20 (NRP 20), pp 251–259

Kerschner H, Ivy-Ochs S (2008) Palaeoclimate from glaciers: examples from the Eastern Alps during the Alpine Lateglacial and early Holocene. Global Planet Change 60:58–71

Korup O (2006) Rock-slope failure and the river long profile. Geology 34:45–48

Korup O (2008) Rock type leaves topographic signature in landslide-dominated mountain ranges. Geophys Res Lett 35:L11402

Korup O, Schlunegger F (2007) Bedrock landsliding, river incision, and transience of geomorphic hillslope-channel coupling: evidence from inner gorges in the Swiss Alps. J Geophys Res 112:F03027

Korup O, Schlunegger F (2009) Rock-type control on erosion-induced uplift, eastern Swiss Alps. Earth Planet Sci Lett 278:278–285

Kubik P, Christl M (2010) ^{10}Be and ^{26}Al measurements at the Zurich 6 MV Tandem AMS facility. Nucl Instrum Methods Phys Res Sect B 268:880–883

Kuhlemann J, Frisch W, Székely B, Dunkl I, Kázmér M (2002) Post-collisional sediment budget history of the Alps: tectonic versus climatic control. Int J Earth Sci (Geologische Rundschau) 91:818–837

Kühni A, Pfiffner OA (2001) The relief of the Swiss Alps and adjacent areas and its relation to lithology and structure: topographic analysis from a 250-m DEM. Geomorphology 41:285–307

Kummerow J, Kind R, Oncken O, Giese P, Ryberg T, Wylegalla K, Scherbaum F, TRANSALP Working Group (2004) A natural and controlled source seismic profile through the Eastern Alps: TRANSALP. Earth Planet Sci Lett 255:115–129

Lippitsch R, Kissling E, Ansorge J (2003) Upper mantle structure beneath the Alpine orogen from high-resolution teleseismic tomography. J Geophys Res B Solid Earth 108. doi:10.1029/2002JB002016

Lyon-Caen H, Molnar P (1989) Constraints on the deep structure and dynamic processes beneath the Alps and adjacent regions from an analysis of gravity anomalies. Geophys J Int 99:19–32

Mancktelow NS (1992) Neogene lateral extension during convergence in the Central Alps: Evidence from interrelated faulting and backfolding around the Simplon pass (Switzerland). Tectonophysics 215:295–317

Molnar P, Lyon-Caen H (1988) Some simple physical aspects of the support, structure, and evolution of mountain belts. Geol Soc Am Spec Pap 218:179–207

Molnar P, Anderson RS, Anderson SP (2007) Tectonics, fracturing of rock, and erosion. J Geophys Res 112:F03014. doi:10.1029/2005JF000433

Montgomery DR (2001) Slope distributions, threshold hillslopes, and steady-state topography. Am J Sci 301:432–454

National Snow and Ice Data Center (1999, updated 2009) World glacier inventory. World Glacier Monitoring Service and National Snow and Ice Data Center/World Data Center for Glaciology. Digital media, Boulder, CO

Neubauer F, Keil M, Windberger M (2007) Initiation and evolution of a major fault-controlled valley: the Enns valley, Eastern Alps. Geophys Res Abstr 9:EGU2007-A-06219

Norton KP, Vanacker V (2009) Effects of terrain smoothing on topographic shielding correction factors for cosmogenic nuclide-derived estimates of basin-averaged denudation rates. Earth Surf Proc Land 34:145–154

Norton KP, von Blanckenburg F, Schlunegger F, Schwab M, Kubik PW (2008) Cosmogenic nuclide-based investigation of spatial erosion and hillslope channel coupling in the transient foreland of the Swiss Alps. Geomorphology 95:474–486

Norton KP, Abbühl LM, Schlunegger F (2010a) Glacial conditioning as an erosional driving force in the Central Alps. Geology 38:655–658. doi:10.1130/G31102.1

Norton KP, von Blanckenburg F, Kubik PW (2010b) Cosmogenic nuclide-derived rates of diffusive and episodic erosion in the glacially sculpted upper Rhone Valley, Swiss Alps. Earth Surf Proc Land 35:651–662. doi:10.1002/esp.1961

Ouimet WB, Whipple KX, Granger DE (2009) Beyond threshold hillslopes: channel adjustment to base-level fall in tectonically active mountain ranges. Geology 37:579–582

Persaud M, Pfiffner OA (2004) Active deformation in the eastern Swiss Alps: post-glacial faults, seismicity and surface uplift. Tectonophysics 385:59–84

Ratschbacher L, Frisch W, Neubauer F, Schmid SM, Neugebauer J (1989) Extension in compressional orogenic belts: the Eastern Alps. Geology 17:404–407

Ratschbacher L, Merle O, Davy P, Cobbold P (1991) Lateral extrusion in the Eastern Alps, part 1: boundary conditions and experiments scaled for gravity. Tectonics 10:245–256. doi:10.1029/90TC02622

Robl J, Stüwe K (2005) Continental collision with finite indenter strength: 2. European Eastern Alps. Tectonics 24. doi:10.1029/2004TC001741

Robl J, Hergarten S, Stüwe K (2008a) Morphological analysis of the drainage system in the Eastern Alps. Tectonophysics 460:263–277

Robl J, Stüwe K, Hergarten S, Evans L (2008b) Extension during continental convergence in the Eastern Alps: the influence of orogen-scale strike-slip faults. Geology 36:603–606

Rosenberg CL, Berger A (2009) On the causes and modes of exhumation and lateral growth of the Alps. Tectonics 28: TC6001. doi:10.1029/2008TC002442

Rosenberg CL, Brun J-P, Cagnard F, Gapais D (2007) Oblique indentation in the Eastern Alps: insights from laboratory experiments. Tectonics 26:TC2003. doi:10.1029/2006TC001960

Ruess D, Höggerl N (2002) Bestimmung rezenter Höhen—und Schwereänderungen in Osterreich. In: Friedl G, Genser J, Handler R, Neubauer F, Steyer H-P (eds) Pangeo Austria, Institut für Geologie und Paläontologie, Universität Salzburg, Salzburg, p 151

Safran EB, Bierman PR, Aalto R, Dunne T, Whipple KX, Caffee M (2005) Erosion rates driven by channel network incision in the Bolivian Andes. Earth Surf Proc Land 30:1007–1024

Schaller M, von Blanckenburg F, Veldkamp A, Tebbens LA, Hovius N, Kubik PW (2002) A 30,000 year record of erosion rates from cosmogenic ^{10}Be in Middle European river terraces. Earth Planet Sci Lett 204:307–320

Schlatter A, Schneider D, Geiger A, Kahle HG (2005) Recent vertical movements from precise levelling in the vicinity of the city of Basel, Switzerland. Int J Earth Sci 94:507–514

Schlunegger F, Schneider H (2005) Relief-rejuvenation and topographic length scales in a fluvial drainage basin, Napf area, Central Switzerland. Geomorphology 69:102–117

Schlunegger F, Simpson G (2002) Possible erosional control on lateral growth of the European Central Alps. Geology 30:907–910

Schmid SM, Kissling E (2000) The arc of the western Alps in the light of geophysical data on deep crustal structure. Tectonics 19:62–85

Schmid M, Aebli HR, Heller F, Zingg A (1989) The role of the Periadriatic Line in the tectonic evolution of the Alps. In: Conference on Alpine tectonics, vol 45. Geological Society Special Publications, London, pp 153–171

Schmid SM, Pfiffner OA, Froitzheim N, Schönborn G, Kissling E (1996) Geophysical-geological transect and tectonic evolution of the Swiss-Italian Alps. Tectonics 15:1036–1064

Schmid SM, Fügenschuh B, Kissling E, Schuster R (2004) TRANSMED transects IV, V and VI: three lithospheric transects across the Alps and their forelands. In: Cavazza W, Roure F, Spakman W, Stampfli GM, Ziegler PA (eds) The TRANSMED atlas: the Mediterranean region from crust to mantle. Springer, Heidelberg

Schwab M, Schlunegger F, Schneider H, Stöckli G, Rieke-Zapp D (2009) Contrasting sediment flux in Val Lumnezia (Graubünden, Eastern Swiss Alps), and implications for landscape development. Swiss J Geosci 102:1661–8726

Schwarb M (2001) The Alpine precipitation climate. Evaluation of a high-resolution analysis scheme using comprehensive rain-gauge data. Züricher Klimaschriften 80

Selverstone J (2005) Are the Alps collapsing? Annu Rev Earth Planet Sci 33:113–132

Snyder NP, Whipple KX, Tucker GE, Merrits DJ (2000) Landscape response to channel forcing: DEM analysis of stream profiles in the Mendocino triple junction region, northern California. Geol Soc Am Bull 112:1250–1263

Snyder NP, Whipple KX, Tucker GE, Merritts DJ (2003) Channel response to tectonic forcing: field analysis of stream morphology and hydrology in the Mendocino triple junction region, northern California. Geomorphology 53:97–127

Stüwe K, Barr TD (1998) On uplift and exhumation during convergence. Tectonics 17:80–88

Tapponnier P, Peltzer G, Armijo R (1986) Collision tectonics, vol 19. Geological Society Special Publications, London, pp 115–157

Vernon AJ, van der Beek PA, Sinclair HD, Rahn MK (2008) Increase in late Neogene denudation of the European Alps confirmed by analysis of a fission-track thermochronology database. Earth Planet Sci Lett 270:316–329

Vernon AJ, van der Beek P, Sinclair HD (2009) Spatial correlation between long-term exhumation rates and present-day forcing parameters in the western European Alps. Geology 37:859–862

von Blanckenburg F (2005) The control mechanisms of erosion and weathering at basin scale from cosmogenic nuclides in river sediment. Earth Planet Sci Lett 237:462–479

von Blanckenburg F, Kagami H, Deutsch A, Wiedenbeck M, Oberli F, Meier M, Barth S, Fischer H (1998) The origin of Alpine plutons along the Periadriatic Lineament. Schweiz Mineral Petrogr Mitt 78:55–66

Vrabec M, Pavlovcic Preseren P, Stopar B (2006) GPS study (1996–2002) of active deformation along the Periadriatic fault system in northeastern Slovenia: tectonic model. Geologica Carpathica 57(1):57–65

Wagner T, Fabel D, Fiebig M, Häuselmann P, Sahy D, Xu S, Stüwe K (2010) Young uplift in the non-glaciated parts of the Eastern Alps. Earth Planet Sci Lett. doi:10.1016/j.epsl.2010.03.034

Weber J, Vrabec M, Pavlovčič-Prešeren P, Dixon T, Jiang Y, Stopar B (2010) GPS-derived motion of the Adriatic microplate from Istria Peninsula and Po Plain sites, and geodynamic implications. Tectonophyics 483:214–222

Whipple KX (2004) Bedrock Rivers and the geomorphology of active orogens. Annu Rev Earth Planet Sci 32:151–185

Whipple KX (2009) The influence of climate on the tectonic evolution of mountain belts. Nat Geosci 2:97–104

Whipple KX, Kirby E, Brocklehurst SH (1999) Geomorphic limits to climate-induced increases in topographic relief. Nature 401: 39–43

Willenbring JK, von Blanckenburg F (2010) Long-term stability of global erosion rates and weathering during late-Cenozoic cooling. Nature 465:211–214. doi:10.1038/nature09044

Willet SD, Schlunegger F, Picotti V (2006) Messinian climate change and erosional destruction of the central European Alps. Geology 34:613–616

Willett SD (2010) Late Neogene erosion of the Alps: a climate driver? Annu Rev Earth Planet Sci 38:409–435

Willett SD, Brandon MT (2002) On steady states in mountain belts. Geology 30:175–178

Willett SD, Slingerland R, Hovius N (2001) Uplift, shortening, and steady state topography in active mountain belts. Am J Sci 301:455–485

Wittmann H, von Blanckenburg F, Kruesmann T, Norton KP, Kubik PW (2007) Relation between rock uplift and denudation from cosmogenic nuclides in river sediment in the Central Alps of Switzerland. J Geophys Res 112:F04010. doi:10.1029/2006JF000729

Wobus C, Whipple KX, Kirby E, Snyder E, Johnson J, Spyropolou K, Crosby B, and Sheehan D (2006) Tectonics from topography: Procedures, promise, and pitfalls. In: Willett SD, Hovius N, Brandon MT, Fisher DM (eds) Tectonics, climate, and landscape evolution: Geological Society of America Special Paper 398, Penrose Conference Series, Geological Society of America, pp 55–74